RSC Advances

This is an *Accepted Manuscript*, which has been through the Royal Society of Chemistry peer review process and has been accepted for publication.

Accepted Manuscripts are published online shortly after acceptance, before technical editing, formatting and proof reading. Using this free service, authors can make their results available to the community, in citable form, before we publish the edited article. This *Accepted Manuscript* will be replaced by the edited, formatted and paginated article as soon as this is available.

You can find more information about *Accepted Manuscripts* in the Information for Authors.

Please note that technical editing may introduce minor changes to the text and/or graphics, which may alter content. The journal's standard Terms & Conditions and the Ethical guidelines still apply. In no event shall the Royal Society of Chemistry be held responsible for any errors or omissions in this *Accepted Manuscript* or any consequences arising from the use of any information it contains.

ROYAL SOCIETY OF CHEMISTRY

www.rsc.org/advances

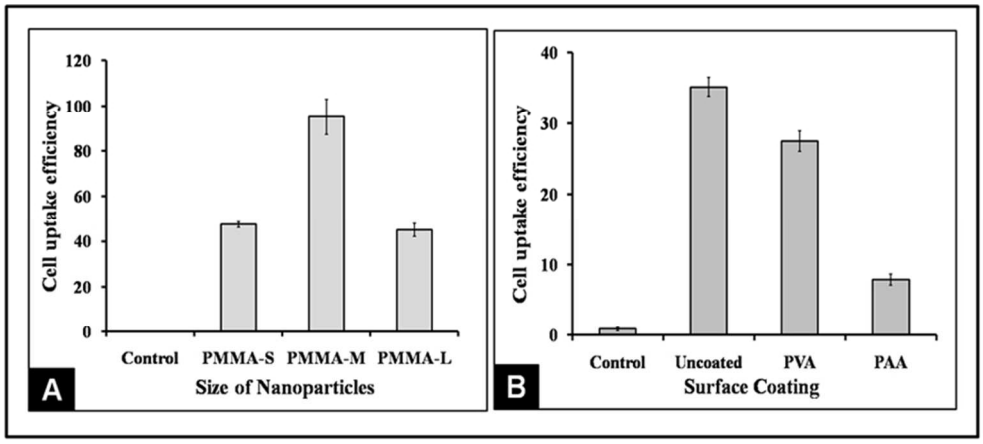

Differential in vitro cellular uptake efficiency of fluorophore-loaded PMMA nanoparticles, with (A) different size, and (B) different surface coating.
76x57mm (300 x 300 DPI)

RSC Advances Accepted Manuscript

Cite this: DOI: 10.1039/c0xx00000x

www.rsc.org/xxxxxx

PAPER

Surface modified PMMA nanoparticles with tunable drug release and cellular uptake

Ridhima Juneja and Indrajit Roy

Received (in XXX, XXX) Xth XXXXXXXXX 20XX, Accepted Xth XXXXXXXXX 20XX

DOI: 10.1039/b000000x

In this manuscript, we report the microemulsion mediated synthesis of fluorophore-doped PMMA nanoparticles, with different size and surface coating, for potential biomedical applications. Size variation was achieved by modulating the amount of co-surfactant n-butanol. After synthesis, their size, surface, and optical properties were evaluated. Nanoencapsulation was found to enhance the stability of the fluorophore against chemically induced quenching. The surface of the nanoparticles was modulated via coating with hydrophilic polymers PAA and PVA. Hydrophilic coating resulted in enhancement of the colloidal stability of these nanoparticles in physiological saline medium. The release pattern of encapsulated fluorophore was found to depend on both the size and surface property of the nanoparticles. Fluorescence bioimaging and fluorescence analysis of lysates of treated cells were used to study the cellular uptake of the nanoparticles. The cellular uptake was also found to depend on both size and surface properties of these nanoparticles. Finally, cell viability (MTS) assay *in vitro* have indicated the absence of cytotoxic effects of these doped nanoparticles. These results underscore the promise of these nanoparticles in non-toxic biomedical applications.

Introduction

Polymeric nanoparticles have been widely used in both therapeutic and diagnostic applications[1,2]. The useful attributes of such nanoparticles in drug delivery are (a) biocompatibility, (b) colloidal stability in physiological medium, (c) ability to encapsulate active agents, such as hydrophobic drugs, (d) targeting to specific cells/tissues, (e) capability of controlled drug release, etc. Their composition, size, and surface properties are critical parameters that determine their biomedical impact. Generally, as most drugs and other active synthetic molecules are poorly water soluble, hydrophobic polymers are well suited for encapsulating such molecules. Polymer hydrophobicity also facilitates their interaction and uptake in cells of interest. However, surface hydrophobicity also may lead to colloidal instability of nanoparticles in the physiological milieu, along with abnormal drug release. Hydrophobic nanoparticles are specifically vulnerable to capture by biological barriers, such as the reticuloendothelial system (RES), mucus, etc. Therefore, appropriate surface modification of these nanoparticles with hydrophilic polymers is necessary.

Poly-methyl methacrylate (PMMA) is a biocompatible polymer which has been widely used in drug delivery applications. This transparent polymeric material possesses several desirable characteristics, such as resistance to chemical hydrolysis, achirality, high permeability for many drugs, lack of toxicity, etc[3]. Since PMMA nanoparticles are non-biodegradable, they have usefulness in bio-distribution and cell-uptake studies. This feature permits their long-term tracking in the physiological milieu, without the contamination of any degradation product[4-6]. The earliest experiments of PMMA as a carrier material were in the field of vaccines, and on beads to fill defects related to surgical resection of chronic osteomyelitis[7-10]. Other biomedical applications of PMMA include its use as a prosthetic material in dental and mandibular corrections and as a permanent implant for intraocular lens following cataract surgery[11]. At present, it is generally accepted that PMMA is a non-toxic polymer as it possesses a good toxicological safety record in biomedical applications. Yet, till date no successful drug delivery system of this polymeric carrier has made its way to the clinic.

There are several shortcomings related to the synthetic procedures of PMMA nanoparticles. Earlier formulations of these nanoparticles used hazardous γ radiations for initiating polymerization. Conventional emulsion as well as microemulsion polymerization techniques suffered from toxicological issues associated with incomplete removal of surfactants and corrosive organic solvents. Similarly, surfactant-free emulsion polymerization (SFEP) technique of PMMA nanoparticle synthesis not only involved the use of γ radiation, but also toxic chelated metal complexes[12] and/or redox couples[13], as catalysts or initiators. Besides toxicity, other shortcomings of synthesized PMMA nanoparticles included size polydispersity, ineffective loading of dye/drug, abnormal drug release and RES capture.

RSC Advances Accepted Manuscript

Herein, we have synthesised fluorophore-doped PMMA nanoparticles via free radical polymerization in the oil-in-water microemulsion medium, using a water insoluble initiator[14-20]. We have observed several improvements in our formulation over other conventional methods, such as size control and monodispersity, easy purification of the nanoparticles with almost complete removal of impurities or any unreacted species, good yield and excellent encapsulation efficiency. This process allowed the fabrication of mono-disperse and colloidally stable nanoparticles. Size control was achieved by variation of the amount of co-surfactant. Post synthesis, all contaminants, such as unreacted monomers, organic solvents, initiators, surfactants, co-surfactants, etc., were completely removed by dialysis and centrifugation. The use of microemulsion medium ensured control over both nanoparticle size and drug loading capacity. The resulting fluorophore-doped nanoparticles were characterized for their size, composition, surface, crystallinity, along with their optical behaviour. The optical stability of the nanoencapsulated fluorophore vis-a-vis that of the free fluorophore was probed. The nanoparticle surface was also modulated via coating with two hydrophilic polymers, namely polyacrylic acid (PAA) and polyvinyl alcohol (PVA). The effect of modulation of nanoparticle surface on their colloidal stability, drug release and cellular uptake was then investigated. Finally, their compatibility with cells *in vitro* was investigated using cell viability assay.

Experimental

Materials:

Surfactant aerosol OT (AOT) was purchased from Across Organics. Co-surfactant n-butanol was obtained from Merck. Monomer methyl methacrylate (MMA) and initiator, Azobisisobutyronitrile (AIBN) were procured from Alfa Aesar. Fluorophore nile red and cell viability (MTT) reagent were obtained from Sigma Aldrich. The following polymers were used for coating: polyvinyl alcohol (PVA) (Mw 61,000), purchased from Aldrich; and poly acrylic acid (PAA) (Mw 5,000) (25% wt solution), purchased from Alfa Aesar. The solvents used during polymerization were purchased from Rankem. Cell culture reagents were obtained from Invitrogen. The lung carcinoma cells lines (A-549) were purchased from ATCC, VA, and cultured according to vendor's instructions. All chemicals were used without any further purification.

Synthesis of PMMA nanoparticles within micellar core:

Polymerization of the monomer MMA was carried out in the hydrophobic core of the oil-in-water microemulsion, with AOT as the surfactant and n-butanol as the co-surfactant. Briefly, 0.22g of AOT was added to a 10mL volume of double distilled water. It was stirred for about 30mins, giving a translucent system. This system was converted to a clear solution via addition of n-butanol (co-surfactant). Three separate batches of nanoparticles were synthesized, corresponding to three different amounts of co-surfactant added (Table 1). For fluorophore encapsulation, 100 ul of nile red in dioxane (15.7mM) was dissolved in each solution. After this, 1:1(v/v) solution of MMA in dioxane (1000 ul) was added dropwise to each solution. Only after the solutions became clear, the initiator AIBN (3-4mg) was added to them. The amounts/concentrations of the various components added are provided in table 1. Each solution, having both the monomer and the initiator in the micellar core, was purged with nitrogen gas for an hour for removal of oxygen, which may interfere with the polymerization process. Polymerization was then carried out at a temperature of 60-70 ^{0}C overnight under nitrogen atmosphere. Each solution turned milky upon completion of polymerization. Purification of the prepared polymeric nanoparticles was carried out via dialysis (cellulose membrane with 12kD cut-off were used) for about 48 hours, followed by centrifugation and washing with water.

PVA/PAA Coating:

After purification of these hydrophobic polymeric nanoparticles, these were coated with hydrophilic polymers for enhanced compatibility with the aqueous physiological system. Two polymers were used for coating purpose, namely polyvinyl alcohol (PVA) and poly acrylic acid (PAA). To 10mL aqueous dispersion of the nanoparticles, excess of PAA (0.5 ml of 2% aqueous solution) was added and the solution was kept on stirring for 1hr. Similar procedure was followed for coating with PVA (0.5 ml of 2% aqueous solution of PVA with 10 ml of aqueous dispersion of nanoparticles). We observed this coating process using salt-induced aggregation and zeta-potential measurements.

Adsorption of flexible, hydrophilic and anionic/neutral polymers at lipophilic surfaces has been studied extensively and is now a well understood phenomenon. These adsorptions take place *via* non-covalent and non-electrostatic physical interactions.[21] PAA has been widely used to stabilize the colloids, which is closely related to the adsorption. This polymeric adsorption is purely a physical process, wherein surface adhereing nature of acrylate groups come into play. On the other hand, the adsorption of PVA is likely to occur *via* non-covalent interpenetration of lipophilic chains of PVA and PMMA. [22]

Batch	MMA:DIOXANE (v/v)	Initiator (mg)	AOT (M)	*Butanol (µL)
A.	1:1	3.00	0.050	500
B.	1:1	3.00	0.050	670
C.	1:1	3.00	0.050	800

Table.1: The amounts/concentrations of the various components used during synthesis of nanoparticles.

Salt-induced aggregation:

The colloidal stability of these nanoparticles, with and without surface coating, was then investigated in physiological saline medium. Briefly, equal volumes of the three systems (uncoated PMMA, PAA-coated PMMA and PVA-coated PMMA solutions) were taken separately. To these, aqueous NaCl solution was added to have a final NaCl concentration of 0.9% (saline

RSC Advances Accepted Manuscript

 This journal is © The Royal Society of Chemistry [year]

solution). The effect of the saline medium on the colloidal stability of these nanoparticles was then observed visually.

Characterization:

The sizes of the polymeric nanoparticles, with variable amount of n-butanol, were determined using transmission electron microscopy (TEM). For TEM, the aqueous dispersions were sonicated and drop-coated and dried to a thin film onto formvar coated 200 mesh copper grids (Ted Pella, USA), followed by imaging in a TECNAI G2-30 U TWIN TEM instrument (FEI, Eindhoven, Netherlands) with an acceleration voltage of 300 kV.

The hydrodynamic diameters of the nanoparticles were further analyzed by dynamic light scattering (DLS) measurements. Here, aqueous dispersed nanoparticle samples were taken in glass cuvettes, and analysed using a NANO-ZS series MALVERN ZETASIZER instrument. A He–Ne laser (wavelength 633 nm, power 4 mW) was used as the light source. The number average hydrodynamic size distribution of the nanoparticles was plotted.

The identification of various functional groups present in the polymeric entity forming the nanoparticles were probed using fourier transform infrared (FTIR) and proton nuclear magnetic resonance (1H NMR) spectroscopies. The FTIR spectra of the samples were recorded on a Perkin Elmer 1600 series Infrared Spectrophotometer. The samples were prepared by dispersion into KBr paste and pressing into a pellet. The IR detection range was 450 to 4500 cm^{-1} with a resolution of 4 cm^{-1}. The NMR spectra were obtained using an NMR apparatus (JEOL) at room temperature in $CDCl_3$, with tetramethylsilane (TMS) as an internal standard.

The optical properties (UV-visible absorption and fluorescence emission spectra) of the various nanoparticulate samples, both with and without doped fluorophore nile-red (NR), were recorded using a Shimadzu UV-1601 spectrophotometer (Shimadzu, Kyoto, Japan) and a Cary Eclipse fluorescence spectrometer (Varian, Palo Alto, CA), respectively.

The stability of the fluorophore NR, both free and nanoencapsulated, was studied using a fluorescence quenching experiment. Here, fixed concentrations of free and nanoencapsulated fluorophores in aqueous medium were treated with various concentrations of the chemical quencher Cu^{2+} (copper sulfate)[23]. Fluorescence emission intensities in the absence (Io) and presence (I) of various quencher concentrations was then measured using the Cary Eclipse fluorescence spectrophotometer. A plot was made with the natural log of (I/Io) versus quencher concentration [Q]. The slope of the plot correlated directly with the magnitude of chemical quenching of the fluorophore.

Release Studies:

The release patterns of the encapsulated fluorophore from the polymeric nanoparticles, with different size and surface properties, were examined by dialyzing them against a solution containing Tween-80 micelles (1% in water) for two weeks. The fluorophore-doped samples investigated were PMMA nanoparticles with three different sizes (PMMA-S, PMMA-M and PMMA-L), each uncoated as well as coated with PVA and PAA. As owing to the low cut-off (12-14 kDa) pore size of the dialysis membrane, only free NR molecules can come out of the membrane. We have estimated the amount of released NR by measuring it's concentration in the bulk solution as a function of time of dialysis. The concentration of NR in the bulk solution was found out using spectrofluorometry, by measuring fluorescence intensity corresponding to emission maxima of NR (515nm). The NR concentrations were estimated from a previously drawn calibration curve involving NR concentration and corresponding fluorescence intensity.

***In vitro* studies:**

The lung carcinoma cells lines (A-549) were grown in DMEM media, supplemented with 10% fetal bovine serum (FBS), 1% antibiotic penicillin/streptomycin, and 1% antifungal Amphotericin B. The cells were maintained at 37 °C, 5% CO_2 in a humidified incubator, as instructed in vendor's manual.

For analyzing cell viability upon treatment with various nanoparticles, one day prior to treatment, the cells were trypsinized and resuspended in fresh media. About 1,00,000 cells/1 mL fresh media were added to each well of a sterilized 24-well plate, and transferred back to the incubator for attachment and overnight growth. Next day, to the cells at a confluency of 70–80%, three different dosages of the various samples were added, mixed by swirling, and transferred back to the incubator. The added samples were PMMA nanoparticles, PMMA nanoparticles coated with PAA/PVA, and PMMA nanoparticles encapsulating fluorophore NR. After three days of incubation, the plate was taken out, the cells in each well washed three times with sterile PBS, and treated with 100 μL of MTT reagent [3-(4,5-dimethylthiazol-2-yl)-2,5-diphenyltetrazolium bromide, (5 mg/mL in PBS)] for 2 hours[24]. The resulting blue-colored formazan crystals were dissolved in DMSO, and the optical density of this solution was recorded at 570 nm using UV–visible spectrophotometry. The optical density of each solution reflected the viability of the cells in each well. The percentage viability of the treated cells were calculated after comparing their optical density with that of non-treated cells (positive control), the later being arbitrarily assigned 100 % viability. The experiment was carried out in triplicates for statistical significance.

For monitoring the uptake of the dye-doped nanoparticles in cells, one day prior to treatment, the cells were seeded in sterilized 6-well plate (2,00,000 cells/2 mL fresh media in each well) and returned to the incubator. Next day, to the cells at a confluency of 70–80%, the doped nanoparticle samples were added, mixed by swirling, and returned to the incubator for two hours. After incubation, the plate was taken out, the cells in each well washed twice with sterile PBS, and fixed by a mixture of methanol and glycerol. The fixed cells were visualized under a fluorescent Nikon TS-100 inverted microscope, and photographed using a Nikon DIGITAL SIGHT DS-Fi1 Camera (Nikon, Japan).

For a quantitative analysis of cellular uptake of fluorescently doped nanoparticles, analysis of fluorescence recovered from lysates of treated cells was carried out. About 1,00,000 cells/1 mL fresh low serum media were added to each well of a sterilized

RSC Advances Accepted Manuscript

24-well plate, and transferred back to the incubator for attachment and overnight growth. Next day, to the cells at a confluency of 70–80%, the nanoparticles of various sizes and surface modification were added in triplicates, mixed by swirling, and transferred back to the incubator. After two hours of incubation, the plates were taken out, and the cells in each well were washed three times with sterile PBS, and treated with 100 µL of cell culture lysis reagent (1% TX-100) and incubated for 30min. After incubation, the cells were scraped with sterile scraper, and then to each well 1mL DMSO was added and mixed well. The contents were then transferred in separate microcentrifuge tubes and were centrifuged at 3000rpm for 5mins. The supernatant was separated and fluorescence analysis was carried out by measuring fluorescence intensity corresponding to emission maxima of NR (515nm).

Results and Discussions:

After synthesis and purification, simple visual observation indicated that the nanoparticles of all the three sizes remained colloidally stable and non-aggregated in salt-free aqueous dispersion. Their size and morphology were determined using transmission electron microscopy (TEM). It could be seen from Figure 1(a-c) that the nanoparticles are spherical and reasonably monodispersed, with tunable size as a function of the amount of co-surfactant. The diameters of the nanoparticles were in the range of 50-70 nm for batch A (PMMA-small, or PMMA-S), 120-150 nm for batch B (PMMA-medium, or PMMA-M), and 170-230 nm for batch C (PMMA-large, or PMMA-L).

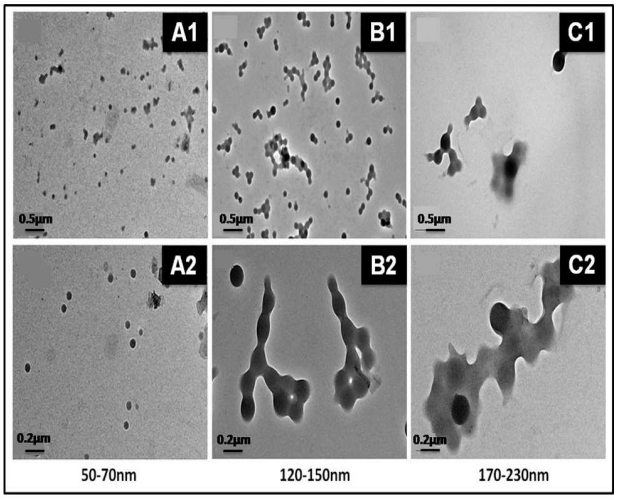

Figure 1: TEM images of PMMA nanoparticles, with added n-butanol (A1,A2) 500µL, (B1,B2) 670µL, and (C1,C2) 800µL. A1, B1, C1: low resolution images; scale bar: 500 nm; A2, B2, C2: high resolution images; scale bar: 200 nm.

Dynamic light scattering (DLS) experiment has been carried out to measure the hydrodynamic diameter of nanoparticles. The results, given in Figure 2 (A-C), also show that the hydrodynamic radii are directly related to the amount of co-surfactant added for nanoparticle synthesis. The radii obtained from DLS studies are 77nm, 132nm, and 206nm (c.a.) for nanoparticles in batch A (PMMA-S), B (PMMA-M), and C (PMMA-L), respectively. The reason why the observed DLS diameter is slightly higher than the TEM diameter lies in the fact that in DLS the hydration layer around the nanoparticles is also counted. Overall, the TEM and DLS data are consistent with each other, and shows reasonable monodispersity in each nanoparticle batch.

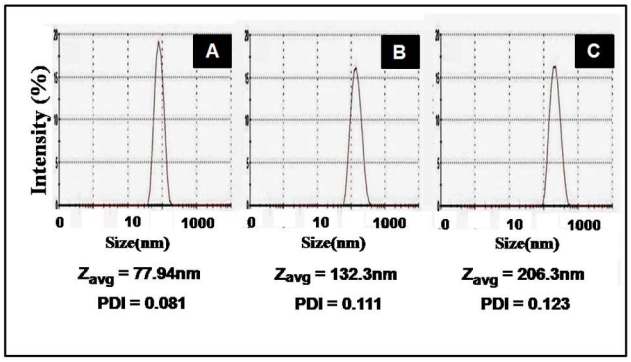

Figure 2: (A-C) DLS graphs showing the average diameter (hydrodynamic diameter) for PMMA nanoparticles with BuOH content being 500µL (A), 670µL (B) and 800µL (C).

The FTIR spectrum of PMMA, given in Figure 3(A), showed absorption bands at 2948 and 1736 cm^{-1} due to -CH_3 asymmetric stretching and C=O stretching, respectively. The vibrational bands between 1420-1450 cm^{-1} are attributed to -CH_2 scissoring and CH_3 asymmetric stretching or deformation of PMMA. The characteristic peak at 1386 cm^{-1} appeared due to -OCH_3 deformation of PMMA. The bands appearing at 1260-1270 and 850-860 cm^{-1} are corresponding to C-O stretching and C-O-C stretching of PMMA, respectively. The absorption bands corresponding to -CH_2 twisting, wagging and rocking modes of PMMA appeared around 1190, 960 and 750 cm^{-1}, respectively. All the bands are consistent with known spectra of PMMA[25]. Figure 3(B) shows the proton NMR spectrum of PMMA. The main features of the 1H-NMR spectra is the peak corresponding to the methoxy hydrogen (-OCH_3) at δ=3.57-3.64, which further verifies the result of FT-IR, confirming the polymerization step.

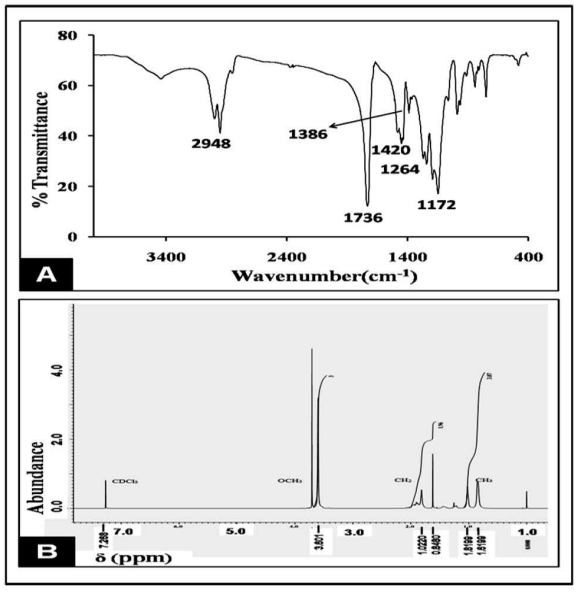

Figure 3: (A) FT-IR spectra, and (B) 1H-NMR spectra of the polymer (PMMA).

RSC Advances Accepted Manuscript

This journal is © The Royal Society of Chemistry [year]

After determining the size and composition, we investigated the colloidal stability of the nanoparticles in physiological conditions by dispersing them in salt-containing (saline) medium. It was observed that uncoated nanoparticles readily aggregated and settled down in the presence of salt (Supplementary data, S1). This aggregation was attributed to the hydrophobicity of the particle surface. Such physiological aggregation is a major factor that impedes the extended circulation of nanoparticles in the body, thereby hampering their therapeutic effectiveness[26]. Therefore, except in some cases of localized (topical) drug delivery, uncoated hydrophobic nanoparticles are poorly suited for drug delivery applications. It is generally known that coating the nanoparticle surface with hydrophilic, biocompatible polymers can prevent their aggregation in physiological environment, therefore enhancing their utility in drug delivery[27, 28]. In our experiment, we have coated the nanoparticle-surface with polyacrylic acid (PAA), as well as polyvinyl alcohol (PVA). These two biologically useful polymers are well known for their ability to coat the surface of hydrophobic nanoparticles [29]. We observed that both the PAA and PVA-coated nanoparticles did not undergo any aggregation in saline solution, contrary to what was found in the case of uncoated nanoparticles (Supplementary data, S1). This observation indicates that hydrophilic coating can enhance the colloidal stability, and hence drug delivery potential in physiological conditions.

Next, the fluorescence emission properties of fluorophore (NR)-doped nanoparticles were studied. As the process of prolonged dialysis results in complete removal of the surfactants, co-surfactants and organic solvents, fluorescence measurements were carried out before and after dialysis for the estimation of NR-loading within the nanoparticles. For comparison, measurements were also carried out on NR dissolved in micelles (non-nanoparticulate control), before and after dialysis.The results are summarized in Figure 4 (A-C). As can be seen from this figure, for all the three samples (PMMA-S, PMMA-M, and PMMA-L), the dilyzed nanoparticles (surfactant free) retained substantial fluorescence. In sharp contrast, in the corresponding micellar samples, there is complete loss of fluorescence upon dialysis. This is because the hydrophobic fluorophore crystallizes and loses its fluorescence properties upon dialysis of the micellar samples. However, surfactant elimination did not substantially affect the NR fluorescence in the nanoparticle samples, as the fluorophore is well dispersed within the hydrophobic polymeric nanomatrix. This experiment proves that the dye is encapsulated and protected within the nanoparticulate core, with substantial retention of its optical properties.

We further investigated whether nanoencapsulation enhances the stability of fluorophores, using a chemically induced fluorescence quenching experiment. From Fig. 5, it is clear that the free fluorophore (dissolved in micelles) is more sensitive to chemical quenching than the nanoencapsulated fluorophore, as the free fluorophore has a steeper fluorescence quenching curve. This result indicates that the optical stability of the fluorophore is enhanced upon nanoencapsulation.

The release profile of encapsulated molecules from carrier nanoparticles is a critical parameter that determines their biomedical utility. Generally, slow-releasing systems have applications in conventional drug delivery, while non-releasing systems are uesful in diagnostic imaging and externally-activated therapies[30]. In this regard, the size and surface coating of nanoparticles are key factors. We investigated the time-dependent release profile of the encapsulated fluorophore from the various nanoparticle samples. The time dependent drug release curves of these samples (NR-doped PMMA-S, PMMA-M and PMMA-L) were probed (Supplementary data, S2). The results are summarized in Table 2. It can be seen that while the percentage drug release is negligible for both uncoated PMMA-S and PMMA-M, it is somewhat discernible (15.2% release in two weeks) for PMMA-L. In general, it can be concluded that uncoated PMMA nanoparticles poorly release encapsulated molecules. Such drug-loaded nanoparticles have usefulness in externally activated therapies following topical administration to diseased sites (e.g. photodynamic therapy of skin cancer). Surface coating with PAA marginally enhanced drug release in PMMA-S and PMMA-M, but not in PMMA-L. While surface coating with PVA substantially enhanced drug release in PMMA-S, but not in

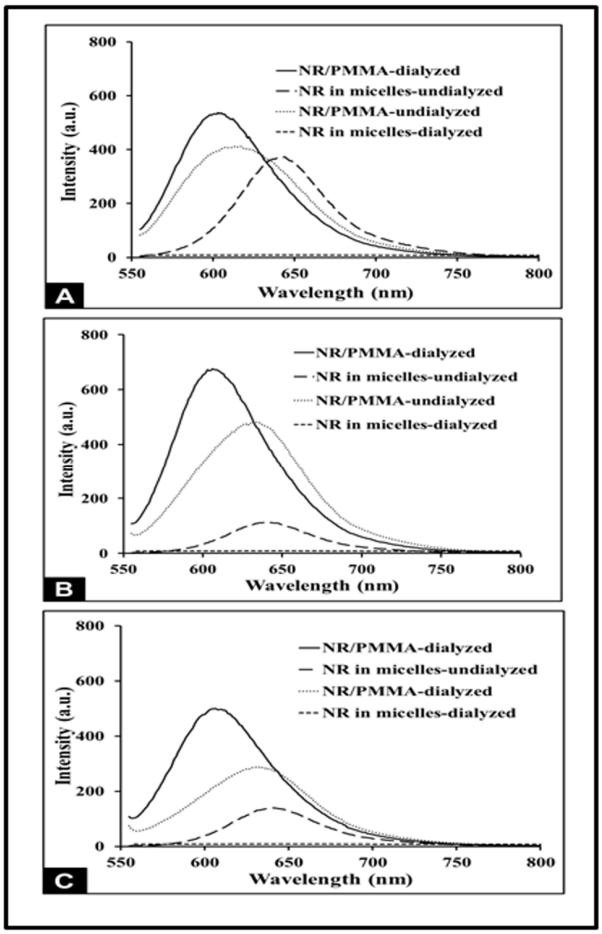

Figure 4 (A-C): Fluorescence emission spectra of NR, (A) dispersed in PMMA-S and dissolved in corresponding micelles; (B) dispersed in PMMA-M and dissolved in corresponding micelles; and (C) dispersed in PMMA-L and dissolved in corresponding micelles. Measurements were carried out before and after dialysis in each case.

RSC Advances Accepted Manuscript

PMMA-M and PMMA-L. Our observation is somewhat consistent with known literature about PMMA, which states that owing to their hydrophobicity uncoated PMMA nanoparticles generally show an incomplete drug release, which can be altered via their surface modification with hydrophilic polymers [31,32]. Strength of the coating can possibly determine the extent of drug release. Our observation also suggest that after hydrophiliccoating, smaller lipophilic nanoparticles are better releasing agents than bigger ones. In general, it can be concluded that both size and surface coating together determines the release profiles of drug-doped nanoparticles.

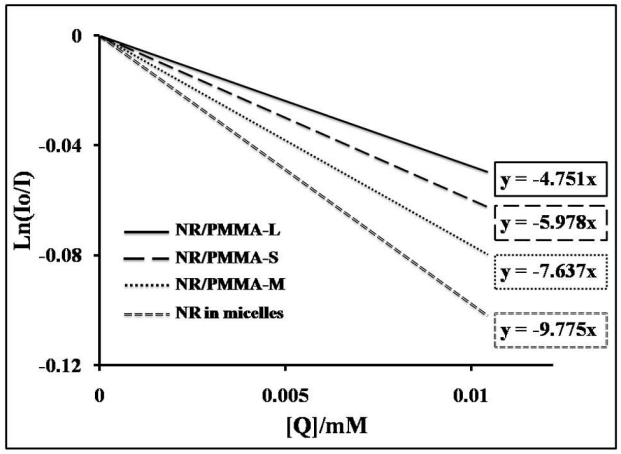

Figure 5: Comparative chemically-induced fluorescence quenching data of fluorophore NR, in free and nanoencapsulated forms.

Batch	Average Size (nm)	Uncoated NPs (%)	PAA coated (%)	PVA coated (%)
PMMA-S	50-70	6.6	33.0	56.0
PMMA-M	130-150	1.6	32.6	7.0
PMMA-L	170-230	15.2	11.0	6.0

Table.2: Percentage Release of the dye from polymeric nanospheres of PMMA (with and without surface modification). The percentage release was studied for a period of two weeks.

Finally, we investigated the interaction of these nanoparticles with cells *in vitro*. First, we studied the efficiency of cellular uptake of these nanoparticles using fluorescence microscopy of nanoparticle-treated cells. The fluorescence of the fluorophore nile red was used to optically track the doped nanoparticle within the cells. Fig. 6A shows the fluorescence image of the treated cells, showing discernible optical signal from the cells (pseudo-coloured in greyscale). The treated cells looked morphologically healthy, as seen from their phase contrast images (Fig. 6B), indicating the non-toxicity of the particles. Control experiments using untreated cells did not result in any optical signal from the cells (data not shown). It may be noted from the above result that efficient optical imaging is possible with a nanoparticle dosage of 150 μg mL^{-1}, which was the lowest dosage used in the cell viability studies. This experiment indicated that the nanoparticles are taken up by the cells. We then quantitatively probed the effect of size and surface variation on this cellular uptake, via estimation of NR fluorescence recovered from the lysates of nanoparticle-treated cells. Figure 6C shows that variation of nanoparticle size resulted in different uptake efficiency, with PMMA-M showing maximum uptake. Figure 6D showed that uncoated nanoparticles showed maximum uptake, which reduced upon coating with hydrophilic polymers PVA and PAA. Hydrophilic coating, although enhances the colloidal stability and RES evasiveness of the lipophilic nanoparticles, also reduces their cellular uptake. It has been shown in literature that cellular uptake, among several factors, depends on the lipophilicity of the nanoparticles [22]. This can be attributed to hydrophobic interaction between the hydrophobic/lipophilic surface of uncoated PMMA nanoparticles and lipophilic cellular membrane. Upon hydrophilic coating, the nanoparticle surface becomes hydrophilic, resulting in diminished cellular interactions.[33] Therefore, it can be concluded that cellular uptake of nanoparticles is both size and surface dependent in case of doped PMMA nanoparticles.

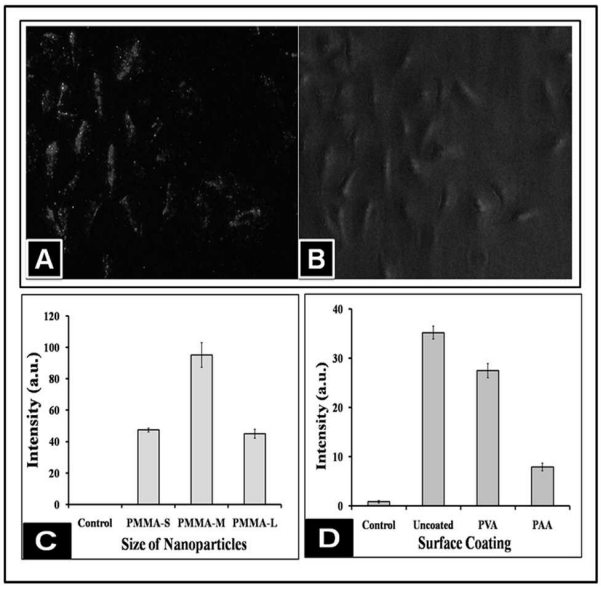

Figure 6: (A) Fluorescence bioimaging data showing image (in greyscale) of cells treated with NR-doped PMMA nanoparticles. (B) Phase contrast image of the same treated cells. (C, D) Fluorescence analysis from lysates of cells treated with NR-doped PMMA nanoparticles with (C) different size, and (D) different surface properties.

In order to learn about the biocompatibility and *in vitro* non-toxicity of the synthesized nanoparticles, cell-viability studies were undertaken, by treating the cell lines with the doped polymeric nanoparticles. It can be seen from figure 7A that after 48 hours of treatment with nanoparticles with three different sizes, the cells remained more than 95 % viable in each case. Thus, all these doped nanoparticles are non-cytotoxic. This non-cytotoxicity also remained preserved upon variation of surface

RSC Advances Accepted Manuscript

 This journal is © The Royal Society of Chemistry [year]

properties of these nanoparticles (Figure 7B). This data demonstrates that doped PMMA nanoparticles exert negligible toxic effect on cells, which remains unaffected upon variation of their size and surface coating. Thus these nanoparticles are well suited for use in biomedical applications.

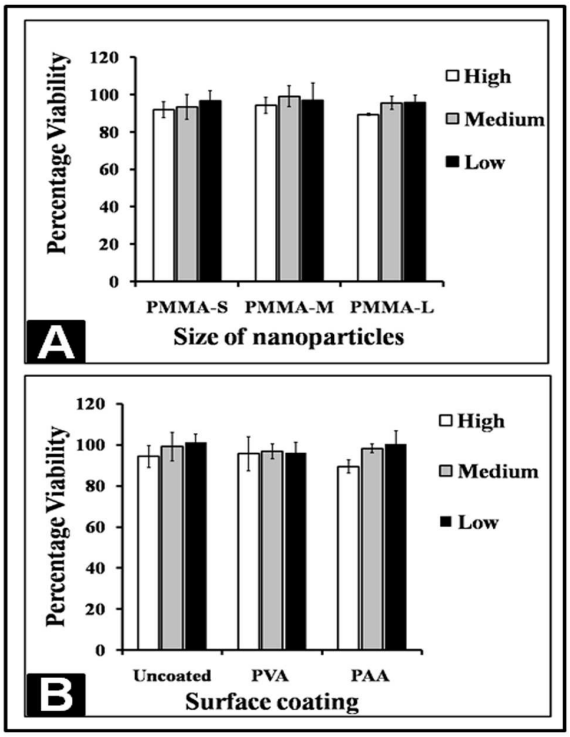

Figure 7: Percentage cell viability of A549 cells, following treatment with doped PMMA nanoparticles of three different (high, medium and low) dosages, with (A) different size, and (B) different surface properties.

Conclusion: Nanoparticles doped with active agents play a critical role in several biomedical applications, which include conventional drug delivery, externally activated therapy, and prolonged bioimaging. Drug-release pattern, cellular uptake, and non-cytotoxicity of nanoparticles are key parameters that determine their usefulness for a specific application. These parameters, in turn, are governed by the composition, size and surface properties of nanoparticles. In this manuscript, we have demonstrated that the drug release pattern and cellular uptake of doped PMMA nanoparticles are modulated by variation in their size and surface coating. Also, all these nanoparticle formulations have been found to be non-toxic to cells *in vitro*. These observations pave the way for exciting potential applications of these nanoparticles, such as in prolonged imaging and externally activated therapy.

Acknowledgements

We are grateful to University of Delhi, India, for providing R&D Grant to support this study. We are also thankful to Mr. Rahul from USIC, University of Delhi, for helping us in recording our TEM images. Finally, we thank Ms. Anuradha for help with *in vitro* studies.

Notes and references

Department of Chemistry, University of Delhi, Delhi-110007, India. Tel: +91-9560721851; E-mail: indrajitroy11@gmail.com

† Electronic Supplementary Information (ESI) available: Salt-induced aggregation effect on nanoparticles, and time dependent release profile curves of fluorophore-doped nanoparticles. See DOI: 10.1039/b000000x/

1. F. Alexis, E. M. Pridgen, R. Langer R and O. C. Farokhzad, *Handb Exp Pharmacol.,* 2010, **197**, 55.
2. S. J. Douglas, S. S. Davis and L. Illum, *Crit Rev Ther Drug Carrier Syst*., 1987, **3**, 233.
3. C. Elvira, A. Fanovich, M. Fernandez, J. Fraile, J. San Roman and C. Domingo, *J Control Release*, 2004, **99**, 231.
4. G. He, Q. Pan and G. L. Rempel, *Macromol. Rapid Commun.*, 2003, **24**, 585.
5. C. Norakankorn, Q. Pan, G. L. Rempel and S. Kiatkamjornwong, *Macromol. Rapid Commun.,* 2007, **28**, 1029.
6. C. Norakankorn, Q. Pan, G. L. Rempel and S. Kiatkamjornwong, *J. Appl. Polym. Sci.*, 2009, **113**, 375.
7. J. Kreuter, R. Mauler, H. Gruschkau and P. Speiser, *Exp. Cell Biol.*, 1976, **44**, 12.
8. J. Kreuter and P. Speiser, *Infect. Immun.*, 1976, **13**, 204.
9. J. Kreuter and P. Speiser, *J. Pharm. Sci.*, 1976, **65**, 1624.
10. J. Kreuter and H. J. Zehnder, *Radiat Eff Defect Solids*, 1978, **35**, 161.
11. K. Klemm, *Zentralbl Chir.*, 1979, **104**, 934.
12. P. K. Sahoo and R. Mohapatra, *European Polymer Journal*, 2003, **39**, 1839.
13. T. P. Chiu and T. M. Don, *Journal of Applied Polymer Science*, 2009, **111**, 388.
14. I. Capek, *Adv. Colloid Interface Sci.*, 1999, **80**, 85.
15. I. Capek, *Adv. Colloid Interface Sci*., 1999, **82**, 253.
16. S. Roy and S. J. Devi, *Appl. Polym. Sci.,* 1996, **62**, 1509.
17. L. M. Gan, C. H. Chew, S. C. Ng and S. E. Loh, *Langmuir*, 1993, **9**, 2799.
18. S. C. Pilcher and W. T. Ford, *Macromolecules*, 1998, **31**, 3454.
19. G. He, Q. Pan and G. L. Rempel, *Ind. Eng. Chem. Res.*, 2007, **46**, 1682.
20. W. Ming, F. N. Jones and S. Fu, *Macromol. Chem. Phys.*, 1998, **199**, 1075.
21. H. Li, B. Liu, X. Zhang, C. Gao, J. Shen and G. Zou. *Langmuir*, 1999, **15**, 2120.
22. S. K. Sahoo, J. Panyam, s. Prabha and V. Labhasetwar. *J. Cont. Rel*., 2002, **82**, 105.
23. B. L. Bales and M. Almgren, *J. Phys. Chem.*, 1995, **99**, 15153.
24. I. Roy, T. Y. Ohulchanskyy, H. E. Pudavar, E. J. Bergey, A. R. Oseroff, J. Morgan, T. J. Dougherty and P. N. Prasad, *J. Am. Chem. Soc.*, 2003, **125**, 7860.
25. K. Kaniappan and S. Latha, *Int. J. Chem. Tech. Res.*, 2011, **3**, 2.
26. K. S. Soppimath, T. M. Aminabhavi, A. R. Kulkarni and W. E. Rudzinski, *J Control Release*, 2001, **70**, 1.
27. K. Knop, R. Hoogenboom, D. Fischer D and U. S. Schubert, *Angew. Chem. Int. Ed.*, 2010, **49**, 6288.
28. S. M. Moghimi, C. J. H. Porter, L. Illum L and S. S. Davis, *Int. J. Pharm.*, 1991, **68**, 121.
29. A. Fink, B. Steitz, A.Finka, J. Salaklang and H. Hofmann, *European Journal of Pharmaceutics and Biopharmaceutics*, 2008, **68**, 129.
30. V. P. Torchilin, *The AAPS Journal*, 2007, **9**, 2.
31. A. Bettencourt and J. Almeida, *Journal of Microencapsulation*, 2012, **9**, 353.
32. M. Feng and P. Li, *J Biomed Mater Res Part A*, 2007, **80,** 184.
33. L. Steffen, P. H. Christoph, A. Benjamin, K. W. Clemens, L. Katharina and M. Volker, *Macromol. Biosci.,* 2010, **10**, 1034.

RSC Advances Accepted Manuscript